

On the PLANCK in-flight antenna beam shape reconstruction using planet transit

P. D. Naselsky^{1,2,4}, O. V. Verkhodanov^{1,3}, P. R. Christensen^{1,4}, and L.-Y. Chiang¹

¹ Theoretical Astrophysics Center, Juliane Maries Vej 30, DK-2100, Copenhagen, Denmark

² Rostov State University, Zorge 5, Rostov-Don, 344090, Russia

³ Special Astrophysical observatory, Nizhnij Arkhyz, Karachaj-Cherkessia, 369167, Russia

⁴ Niels Bohr Institute, Blegdamsvej 17, DK-2100 Copenhagen, Denmark

Received / Accepted

Abstract. An abstract should be given

The calibration of the in-flight antenna beam shape and possible beam degradation is one of the most crucial tasks for the upcoming PLANCK mission. We examine several effects which could significantly act on the in-flight main beam calibration using planet transit: the problems of the variability of Jupiter flux, the antenna temperature and passing of the planets through the main beam. We estimate these effects on the antenna beam shape calibration and calculate the limits on the main beam and far sidelobe measurements, using Jupiter and Saturn. We also discuss possible effects of degradation of the mirror surfaces and specify corresponding parameters which can help us to determine this effect.

Key words. Cosmology: cosmic microwave background — Space vehicles — cosmology: observations — Methods: data analysis — beam restoration — Solar System: general

1. Introduction

The ESA PLANCK Surveyor¹ is designed to image the whole sky of the Cosmic Microwave Background (CMB) radiation with unprecedented sensitivity ($\Delta T/T \sim 2 \times 10^{-6}$) and angular resolution (down to 5') at 9 frequencies: 30, 44, 70, 100, 143, 217, 353, 545, 857 GHz at Low Frequency Instrument (LFI) (Mandolesi et al. 1998) and High Frequency Instrument (HFI) (Puget et al. 1998).

To achieve this high sensitivity and resolution, it is necessary to carefully account for all potential systematic features in the data (Bersanelli & Lamarre 2001).

One of the systematic effects is related to the in-flight antenna beam shape and its reconstruction. Apart from

the need to acquire the radiation pattern of the antenna beam before flight, the calibration of the in-flight antenna beam shape is one of the key components for achieving the scientific goals of the PLANCK mission. This problem has been considered by different PLANCK groups (De Maagt, Polegre and Crone 1998; Burigana et al. 1997, 2001; Chiang et al. 2002a).

The accuracy of the CMB anisotropy C_ℓ estimation will be affected, among other experiment parameters, by our ignorance of the in-flight antenna beam shape of the main beam and far sidelobes, and possible degradation of the mirror surface shapes. During the scanning of PLANCK mission the antenna beam moves across the sky, meaning that antenna beam response is a function of time. After pixelization of the time-ordered data the position of each pixel on the pixelized CMB map is directly related to some data points in the time stream. It is therefore necessary to obtain the information about the in-flight beam shape, its inclination and the location of the beam center relative to each pixel, in order to improve the model of the in-flight main beam shape as well as in the far sidelobe region.

To tackle this issue, Burigana et al. (2001) have suggested a method which uses planet transit to reconstruct the in-flight beam shape. These planet crossings can help the in-flight beam recovery down to $-25 \div 32.5$ dB at 30 GHz. They also showed that the main beam pattern can be described by the bivariate Gaussian approximation. Recently Chiang et al. (2002a) proposed another method for the beam shape estimation based on the interplay of amplitudes and phases of the sky signal and instrumental noise. This method is useful in extraction of the antenna main beam shape down to $-7 \div 10$ dB, and does not need a strong radio source shape calibration. These methods have laid a base for the determination of both the in-flight antenna beam shape and its variations during observations.

¹ <http://astro.estec.esa.nl/SA-general/Projects/Planck/>

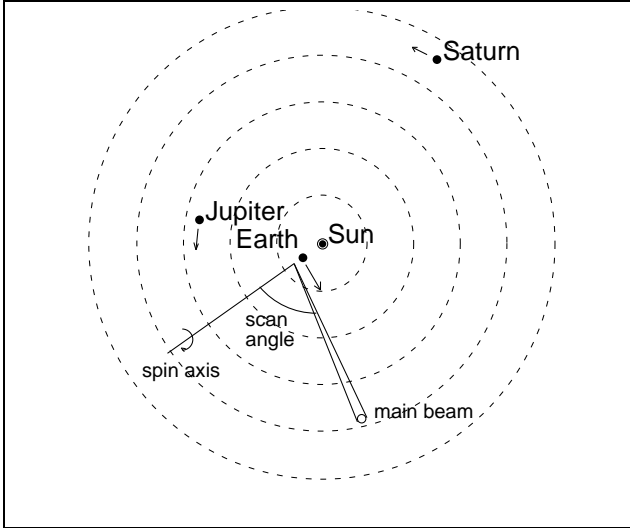


Fig. 1. Positions of Jupiter and Saturn at the beginning of PLANCK mission. The radius of each concentric circle is differed by 2 AU.

The aim of this paper is to re-examine in details the proposed method of the in-flight antenna shape reconstruction by planet crossing (Burigana et al. 2001) in order to estimate possible beam degradation effects. The method, based on Jupiter and Saturn observations, has some subtleties needed to be addressed such as the temporal and frequency variations of Jupiter flux and passing of the planets through the main beam.

This paper is arranged as follows. In Section 2 we describe the PLANCK scan strategy in relation to planet observations, and the beam definitions. In Section 3 we discuss the in-flight beam calibration using planet transit. We concentrate in Section 4 on the effects in beam calibration due to fluctuation of Jupiter's flux density. In Section 5 we discuss variations arising from the distance to the planets and from the scan strategy. Conclusion is in Section 6.

2. Scan strategy and the beam problem

The proposed scan strategy (De Maagt, Polegre and Crone 1998) for PLANCK mission is a whole sky scanning with the satellite orbiting around the L2 Lagrangian point of the Earth–Sun system. The satellite spin–axis will be pointed in the anti-Sun direction and will have a tilt to the ecliptic plane by 10° . The telescope optical angle is inclined by 85° to the spin–axis. The telescope will scan the same circle 60 times around the spin–axis at 1 r.p.m.. Each hour the spin–axis is stepped along the ecliptic plane by $2.5'$. The operational duration is approximately 15 months.

2.1. Planet observations

According to the present schedule, the launch of the satellite is planned in February 2007 and the flight to the L2 point will take approximately six months. To construct the L2, Earth, Jupiter and Saturn orbiting around the Sun, we

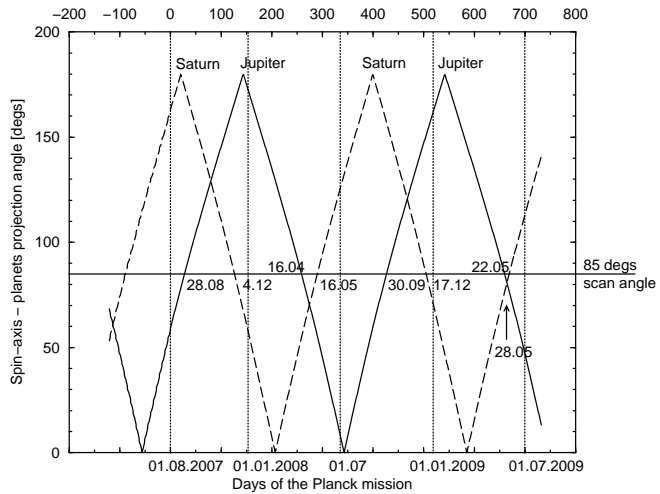


Fig. 2. Transit of Jupiter and Saturn through a scan angle of 85° . The solid and dash curves represent Jupiter and Saturn's paths, respectively. The upper horizontal axis is in days annotated origin set on 01.08.2007.

use the planets ephemerides calculation procedure of the XEphem 3.5.2 software by Downey (2002) (see Fig. 1).

As mentioned above, the scan angle is assigned to be 85° . Assuming the beginning of the mission on the 1st of August 2007, in 15 months Jupiter will cross the main beam direction 3 times on the dates of 28.08.2007, 16.04.2008 and 30.09.2008 with an accuracy of ± 1.5 day, mainly due to tilt and starting conditions, whereas Saturn will cross the main beam 2 times on the dates of 04.12.2007 and 16.05.2008 (Fig. 2).

As shown in Fig. 2, the antenna beam shape calibrations using Jupiter and Saturn can only be realized for 3 + 2 times during the mission, and with a few different time intervals between each planet crossing. These “windows” provide us the possibility to estimate degradation of the antenna main beam shape from the long time frequencies (up to 15 months) to the short frequencies (about 10 days).² For continuous calibration of the main beam area, therefore, it is necessary to use the method by Chiang et al. (2002a) to reconstruct its ellipticity and orientation in the data analysis.

2.2. Inclination of the planets to the ecliptic plane

We make our estimation of the planet transit for the ecliptic plane projection. However, the planets have ecliptic latitude different from zero. The maximum inclinations are $48'$ for Jupiter and $\sim 2^\circ$ for Saturn (the detailed calculation for each planet crossing is in Table 2). Here we

² The interesting point of the track crossing between Jupiter and Saturn near the scan-angle on 28.05.2009 allows us to discuss the possibility of the simultaneous observations of two planets in one scan. However, to make such observations we need to have a scan angle about 80° . Otherwise, these transits can be used to test far sidelobes of the beam.

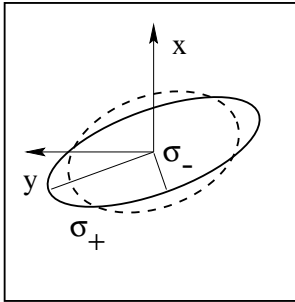
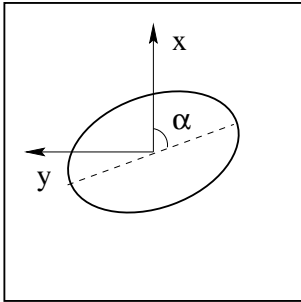


Fig. 3. Beam degradation parameters. The left panel illustrates the orientation angle of the beam and the right panel shows σ_- and σ_+ , the minor and major axis of the elliptical main beam.

note that this problem is not essential for our case but is similar to the tilt projection problem discussed below.

According to the scan strategy proposals the spin-axis can have a tilt to the ecliptic plane at about 10° . This means that usual ecliptic projection of scan angle will be narrower and we shall observe Jupiter in another days with another antenna temperatures. The scan projection ψ of the scan angle α for the tilt angle ϕ can be calculated as

$$\tan \psi = \tan \phi \cos \alpha, \quad (1)$$

which gives us $\psi = 84.92^\circ$, for $\alpha = 85^\circ$ and $\phi = 10^\circ$. This difference is within $5'$, indicating that the projections of the planet trajectories and the tilt of axis will not interfere with our estimates.

2.3. Beam descriptions and its variations due to mirror degradation

The PLANCK “antenna beam” is usually referred to as the physical model of the antenna response and its ground-based verification before the flight, and the *in-flight* antenna beam as the beam reconstructed during flight, which is crucial for possible beam degradation estimation. The *in-flight* antenna beam plays a significant role in the C_ℓ estimation as well as in the extra-galactic point source extraction (Chiang et al. 2002b).

Physics optics calculations have shown that the main beam are roughly elliptical (Mandolesi et al. 2000; Burigana et al. 2001), so we can approximate the antenna pattern as a bivariate Gaussian beam. The geometrical property of the beam in the time domain can be described as follows. We denote by x_0 and y_0 the position of the beam in a coordinate system fixed to the detector with x in scan direction and y perpendicular to x and the beam axis. Then the beam shape can be written as

$$B_t(\mathbf{x} - \mathbf{x}_t) = \exp \left[-\frac{1}{2} (\mathbf{U} \mathbf{U}^T)^T \mathbf{D}^{-1} (\mathbf{U} \mathbf{U}^T) \right], \quad (2)$$

with

$$\mathbf{U} = \begin{pmatrix} x - x_0 \\ y - y_0 \end{pmatrix}, \quad (3)$$

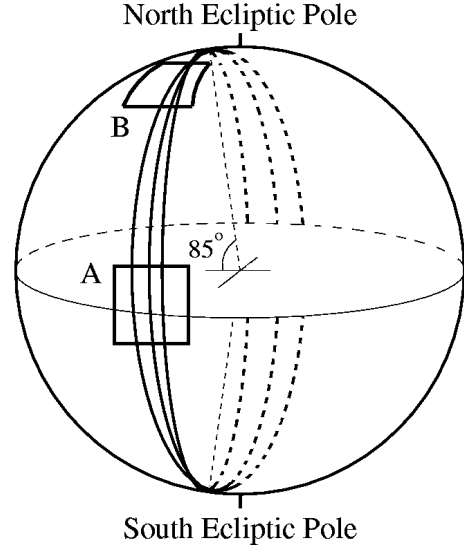


Fig. 4. The PLANCK scan strategy. The square A is located at the parallel scan area, where the planets can be found. The square B has crossing(s) of the circular scans.

where \mathbf{R} is the rotation matrix which describes the inclination of the elliptical beam,

$$\mathbf{R} = \begin{pmatrix} \cos \alpha & \sin \alpha \\ -\sin \alpha & \cos \alpha \end{pmatrix}, \quad (4)$$

with α being the orientation angle between x axis and the major axis of the ellipse. The \mathbf{D} matrix denotes the beam width along the ellipse major axis, which can be expressed as

$$\mathbf{D} = \begin{pmatrix} \sigma_+^2 & 0 \\ 0 & \sigma_-^2 \end{pmatrix}. \quad (5)$$

If, during the routine operation, the mirror surfaces are slightly perturbed (deformed), it is necessary to conduct detailed investigation on the corresponding degradation of the antenna beam shapes, using Jupiter and Saturn transits as suggested by Burigana et al. (2001).³ In general, beam degradation can be described with 3 parameters as illustrated in Fig. 3. First of all, the mean beam width is a function of time,

$$\frac{1}{2}(\sigma_-^2 + \sigma_+^2) \equiv \sigma^2 = \sigma^2(t), \quad (6)$$

where σ_- and σ_+ are the minor and major axis of the elliptical main beam. The orientation angle α between the scan direction and the major axis of the elliptical main beam can also be a function of time, i.e.,

$$\alpha \equiv \alpha(t). \quad (7)$$

and so can the ellipticity ratio of the beam

$$\frac{\sigma_+}{\sigma_-} = \rho \equiv \rho(t). \quad (8)$$

We can use these 3 parameters as the indicators of the degradation level of the *in-flight* antenna beam.

³ As we will see in the next section, Jupiter flux fluctuation could mimic *in-flight* beam degradation effect as well.

3. Planet transits and the pixel domain

Following Burigana et al. (2001), we can specify the in-flight PLANCK antenna beam shape model by using Jupiter as a “standard candle” for calibration. For the PLANCK (both LFI and HFI) frequency range we can model the Jupiter contribution to the resulting $\Delta T(\mathbf{r})$ sky temperature in some direction \mathbf{r} as

$$\Delta T_J(\mathbf{r}) = \frac{S_J(\nu, t)}{2k} \left(\frac{hc}{kT_{\text{CMB}}} \right)^2 \left[\frac{2 \sinh(\eta/2)}{\eta^2} \right]^2 \delta(\mathbf{r}_J, \mathbf{r}), \quad (9)$$

where \mathbf{r} and \mathbf{r}_J are the unit vectors in the corresponding direction on the sky and Jupiter’s location in a given coordinate system respectively, $\delta(\mathbf{r}_J, \mathbf{r})$ is a Dirac delta function, S_J is the Jupiter flux, T_{CMB} , h , k and c are the CMB temperature, Planck constant, Boltzmann constant, and speed of light, respectively, and $\eta = h\nu/kT_{\text{CMB}}$.

Each observed time-ordered subscan m_t^i that includes Jupiter image is related to $\Delta T_J(\mathbf{r})$ from Eq. (9) through a convolution with the antenna beam function $B(\mathbf{r}, \mathbf{r}')$ (see Chiang et al. 2002a)

$$y_t^i = d_t^i + n_t^i \quad (10)$$

where

$$d_t^i = \Delta T_J[\mathbf{r}(t)] \otimes B[\mathbf{r}(t^i), \mathbf{r}(t)], \quad (11)$$

where \otimes denotes convolution, and n_t^i now is the CMB signal plus all the foregrounds and the instrumental noise. The index i marks the i -th subscan with the same orientation of the spin-axis of the satellite.

Using all $i \in [1, N]$ subscans, where N is the total number of the subscans, we can define the circular scan as some linear transformation of the d_t^i :

$$d_t = \mathbf{A} \mathbf{d}^i, \quad (12)$$

where $\mathbf{d}^i = \{d_t^i\}$ is the data vector, and \mathbf{A} is the matrix of the transformation. Eq. (12) gives us the relation of a single circular scan for a fixed orientation of the spin-axis. For simple summation of the subscans we obtain $d_t = (1/N) \sum_i d_t^i$. Below we shall use the circular scan as a basic element for the map-making algorithm taking into account that the variance of the instrumental noise for such a scan is expected to be $\sim N^{-1/2}$ times smaller than for each subscan, if the instrumental noise is pure white noise. For all circular scans we can define the vector of the time-ordered data $\mathbf{y} = \mathbf{M} \mathbf{s} + \mathbf{n}$, where \mathbf{M} is the corresponding map-making matrix, \mathbf{s} denotes the pixelized map and \mathbf{n} is the noise vector (Tegmark 1996). It is worth noting that for the in-flight antenna beam shape reconstruction by using Jupiter and Saturn images, we do not need to construct whole sky maps, because the -40 dB limit of the expected PLANCK antenna beam shape corresponds to angular scale $\theta_{\text{fs}} \sim 5$ degrees at 30 GHz LFI,⁴ and for that purpose we can use the flat sky approximation centered around Jupiter image (Fig. 4), and apply

⁴ For LFI+HFI frequency range this scale corresponds to the minimum.

the method by Chiang et al. (2002a). Furthermore, this assumption allows us to use a linear map-making algorithm (see Tegmark 1996), which is similar, for example, to the COBE pixelization scheme.⁵

The signal in each pixel of the map \mathbf{s} is then (Tegmark 1996)

$$\mathbf{s} = \mathbf{W} \mathbf{y}, \quad (13)$$

where \mathbf{W} is corresponding matrix, which depends on the scan strategy of the PLANCK experiment. For example, for the simplest COBE pixelization we can use $\mathbf{W} = [\mathbf{M}^T \mathbf{N}^{-1} \mathbf{M}]^{-1} \mathbf{M}^T \mathbf{N}^{-1}$, where $\mathbf{N} = \langle \mathbf{n} \mathbf{n}^T \rangle$ is the noise covariance matrix.⁶

Let us go back to the single circular scan. As seen from Eq. (9) and Eq. (11), for the simple average of the subscans ($\mathbf{A} \rightarrow 1/N \sum_i$) the Jupiter’s image after beam convolution in a circular scan should be

$$d_t = \frac{1}{2kN} \left[\frac{2 \sinh(\eta/2) hc}{kT_{\text{CMB}} \eta^2} \right]^2 \sum_i \sum_{t'} S_J(\nu, t'_i) B_t(\boldsymbol{\theta}_i), \quad (14)$$

where $\boldsymbol{\theta}_i = \mathbf{r}'(t'_i) - \mathbf{r}(t_{J,i})$, $t_{J,i}$ is the Jupiter location in the i -th subscan and B_t denotes the beam shape in each subscan. As one can see from Eq. (13) and Eq. (14), in the pixelized map the pixels containing Jupiter image are related to the B_t and $S_J(\nu, t'_i)$ and can be denoted as follows,

$$\mathbf{s} \propto \mathbf{W} S_J(\nu, t'_i) B_t(\boldsymbol{\theta}_i). \quad (15)$$

Therefore, for the definition of the antenna beam shape in the pixel domain, we can specify some possible sources of uncertainties from Eq. (15).

Before focusing on the two categories of variabilities in beam calibration in the next two sections, we would like to briefly mention the uncertainty which is related to the location of Jupiter,

$$\mathbf{r}(t_{J,i}) = \bar{\mathbf{r}}(t_{J,i}) + \Delta \mathbf{r}(t_{J,i}) = \bar{\mathbf{r}}(t_{J,i})(1 + \delta_r), \quad (16)$$

where $\bar{\mathbf{r}}(t_{J,i})$ indicates the average location and $\Delta \mathbf{r}(t_{J,i})$ corresponds to the fluctuation of Jupiter’s location. Generally speaking, this source is related to the pointing accuracy of the PLANCK experiment. It is natural to assume that $\langle \Delta \mathbf{r}(t_{J,i}) \rangle = 0$, but $\langle |\Delta \mathbf{r}(t_{J,i})|^2 \rangle \neq 0$.

4. Variability of Jupiter flux on the beam calibration

The fluctuations of Jupiter flux can be crucial for the in-flight antenna beam shape reconstruction scheme. The

⁵ Note that for estimations of the in-flight beam distortions caused by $1/f$ noise, foreground contaminations and so on, Burigana et al. (2001) have to use the whole sky map for the $1/f$ noise removal.

⁶ Note that we can use any modification of pixelization without loss of information.

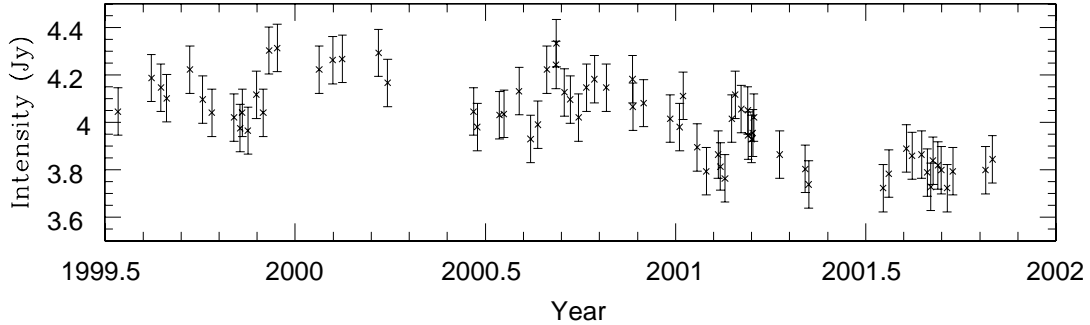


Fig. 5. Variability of the flux density of synchrotron radiation at 4.04 AU from Jupiter at 13 cm wavelength (2.3 GHz) (re-produced from Bolton et al. 2002).

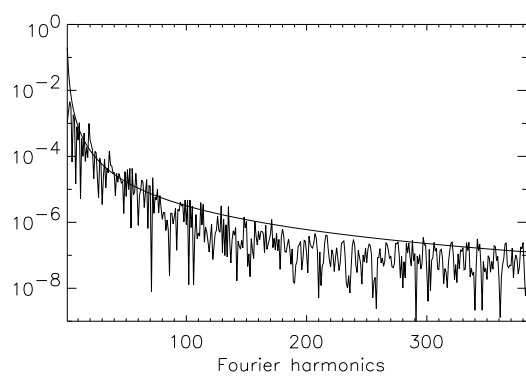


Fig. 6. The power spectrum of the flux density from Jupiter at 13 cm wavelength, which is produced by linear interpolation in the parts of the intervals in Fig. 5 where data are not available. The fitted curve is described by the power law $P(k) \propto k^{-2.4}$.

temporal variations in Jupiter flux can be expressed as the constant flux $\bar{S}_J(\nu)$, and a fluctuating part $\Delta S_J(\nu, t)$,

$$S_J(\nu, t) = \bar{S}_J(\nu) + \Delta S_J(\nu, t) = \bar{S}_J(\nu)[1 + \delta_S(t)]. \quad (17)$$

Returning to Eq. (13) and Eq. (14) in order to define the beam shape properties in the pixel domain, we will assume $\langle \Delta r(t_{J,i}) \rangle = 0$ (so that in Eq. (16) $\delta_r = 0$). The pixelized beam can be obtained from the subscans including Jupiter image as follows (Wu et al. 2001):

$$B_p(\gamma) = \sum_{t \in p} \sum_i \sum_{t'_i} W[1 + \delta_S(\nu, t'_i)] B_t(\theta_i), \quad (18)$$

where γ is the angle between the pixels, which correspond to the Jupiter location in a map and position of each different pixel. Possible variation of Jupiter flux produces an additional source of peculiarities in the pixelized beam shape definition proportional to $1 + \delta_S(t)$.

4.1. Characteristic time scales

There are 3 characteristic time scales related to the PLANCK scan strategy. For each subscan of 1 r.p.m. the time scale is $T_{\text{sub}} \simeq 1$ minute. The next time scale is that for a circular scan $T_{\text{cir}} = 60$ minutes, which is the time interval for data accumulation in one circular scan with a fixed orientation of the spin-axis. In terms of order of magnitude, T_{cir} scale can be used for estimation of the characteristic time scale for the signal variation in one pixel around the main beam area. Another time scale is related to the scale of the far sidelobes $T_{\text{FS}} \simeq \theta_{\text{FS}}/1^\circ$ days, where θ_{FS} is the angular measure subtended by the far sidelobes of the beam. For example, for the LFI 30 GHz channel, the threshold of -30 dB subtends the angular scale $\theta_{\text{FS}} \simeq 1.5$ degrees (Burigana et al. 2001) and thus $T_{\text{FS}} \simeq 1.5$ days. The high-frequency fluctuations of the Jupiter flux which corresponds to the time scales T_{sub} , T_{cir} and T_{FS} are thus very important for the in-flight antenna beam shape reconstruction and may require more detailed investigations, for example by ground-based telescopes. These time scales also indicate that all irregularities of Jupiter flux for $T \geq T_{\text{FS}}$ correspond to long-term variations and could mimic a beam shape degradation effect.

Unfortunately, we do not know exactly the properties of temporal variations in Jupiter flux at the PLANCK frequency range 30-857 GHz. The information about Jupiter flux variability available in the literature that is nearest to LFI frequency range is at 2.3 GHz, which is related to synchrotron emission from the Jupiter magnetic belts.

Fig. 5 shows the variation of the flux density of synchrotron radiation from Jupiter at 2.3 GHz, reproduced from Bolton et al. (2002). The interval of measurement is one day, so any fluctuation shorter than 1 day is yet to be measured. In Fig. 6 we show the power spectrum of Fig. 5, which is produced from linear interpolation in the part of intervals where data are not available.

The temporal variation that can significantly distort the beam reconstruction for the 30 GHz channel is between 2.4 hours and 1.5 days, the PLANCK crossing time

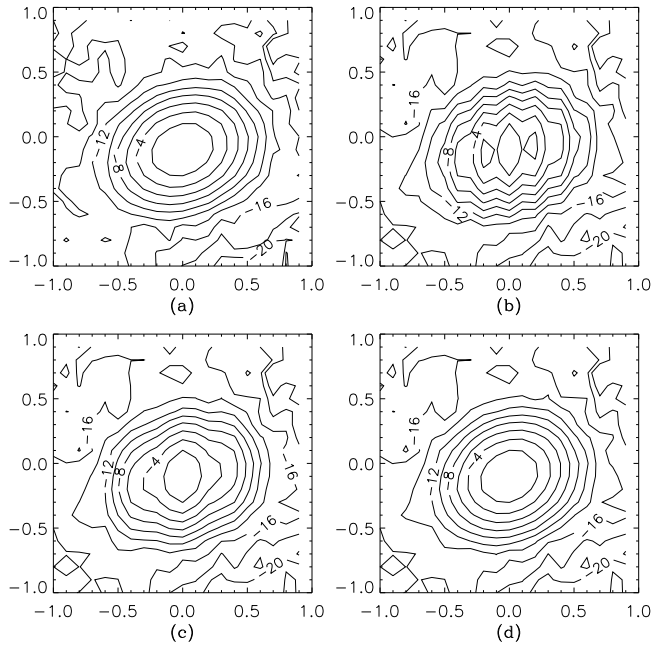
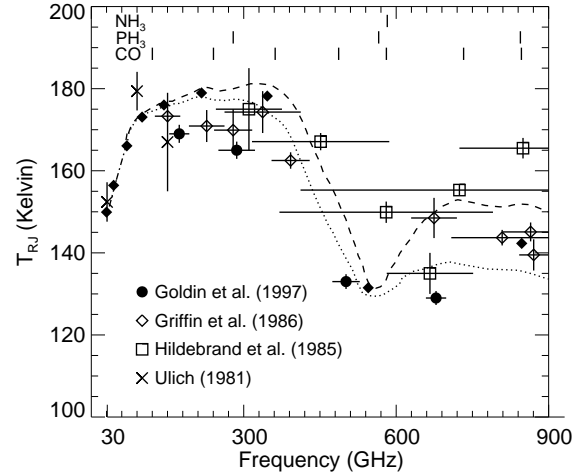


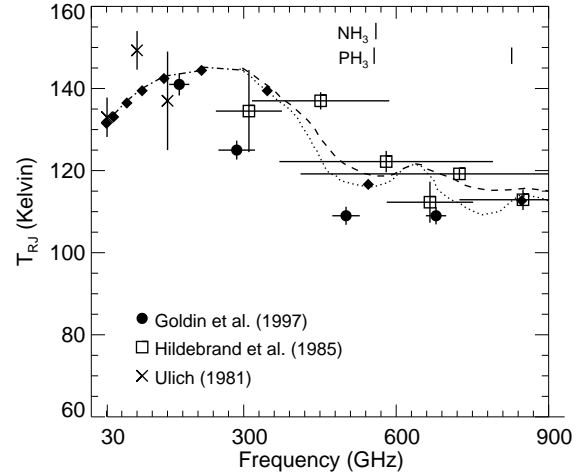
Fig. 7. Simulation on beam reconstruction with variation of Jupiter flux. We simulate LFI 30 GHz channel (FWHM = 33' with ellipticity ratio = 1.3) with σ_{CMB} and pixel noise σ_{pix} equal 3×10^{-5} and 8×10^{-6} , respectively. Panel (a) is without Jupiter flux variation, (b) with Jupiter flux varying with period of 4.8 hours, (c) 10 hours (the rotation period of Jupiter) and (d) 1.5 days (the PLANCK crossing time of Jupiter). The contour lines are annotated in dB.

of Jupiter. Variation period of Jupiter flux shorter than 2.4 hours would be smeared out after pixelization at this channel due to scan strategy and beam shape properties. For variation period longer than 1.5 days, the distortion is much less.

In Fig. 7 we show simulated beam reconstructions at the LFI 30 GHz channel due to possible Jupiter flux variations. According to Eq. (17), if $\delta_S(t)$ is of a random process, in Fourier domain it should be characterized by the power spectrum. We will assume that for Jupiter atmospheric emission the power $\delta_S(t)$ -fluctuations should have a form $P(\omega) \simeq a\omega^{-n} + b$, where a and b are constant. For illustration we will use the same values of a and b -parameters as for the synchrotron emission discussed above. in Fig. 6. The flatness of the power spectrum at large Fourier modes in Fig. 6 allows us to assume the same amplitude of the variation for different periods. Panel (a) is the reconstructed image without variation in Jupiter flux, (b), (c) and (d) are with flux fluctuation of variation period equal 4.8 hours, 10 hours, and 1.5 days, respectively. The period of 10 hours corresponds to that of Jupiter rotation. The amplitude of the variations is assumed to be 20%. We can see clearly that the orientation of the main beam changes due to the fluctuation of Jupiter flux.



(a)



(b)

Fig. 8. The millimeter and sub-millimeter spectrum of Jupiter (top) and Saturn (bottom) (reproduced from Goldin et al. 1997). The filled diamond denotes the fluxes calculated in this work according to the model at the 9 observing frequencies in the PLANCK experiment. Note that the first strong dips in the spectra coincide around PLANCK 545 GHz observing channel.

4.2. Millimeter spectra of the planets and their variations at different frequencies

To estimate the effects of the flux density variation of the planets, we have to look into their radio spectra. The total Jupiter radio spectrum consists of the following two components (Burke & Franklin 1955): the low radio frequency part, which is related with the synchrotron emission from energetic electrons spiraling in Jupiter's magnetic field,

and the high radio frequency part, which corresponds to the thermal atmospheric emission.

The synchrotron emission dominates at the frequency range $\nu \leq 10$ GHz while at $\nu \geq 30$ GHz the Jupiter radio flux is determined by the atmospheric emission. Let us firstly describe the contribution of the synchrotron emission and its variability to the $\delta_S(t_J)$ parameter for the LFI 30 GHz channel. Recent simultaneous observations with the Cassini spacecraft, The Galileo spacecraft and the VLA in the centimeter wavelength range have been made (Gurnett et al. 2002; Bolton et al. 2002). As was shown by Gurnett et al. (2002), there is a strong influence of solar wind on Jupiter's magnetosphere. When interplanetary shocks propagate outwards from the Sun and reach Jupiter, they compress and re-configure the magnetosphere, producing a strong magnetic field and electron acceleration. The $\sim 10\%$ variation with a variability of about 0.5 Jy per month of the 13 cm flux from Jupiter observed by Bolton et al. (2002), and shown in Fig. 5, may most likely be due to such an effect. This value would be used as an upper limit in our estimations. For the PLANCK antenna beam shape reconstruction we need, as shown earlier, to know the variability of the Jupiter flux at the time scale $T_{\text{cir}} \sim 1 \div 2$ days, to obtain the lower limit of the variation for the PLANCK frequency range 30-857 GHz. Obviously, the synchrotron emission is important, in principle, only for 30 GHz channel and it determines the lower limit of the Jupiter flux variation, if the atmosphere emission does not produce any fluctuations of the flux at 30 GHz band. We plot in Fig. 6 the power spectrum of the 13 cm synchrotron flux variability. From this spectrum we find the limit $\Delta_{\text{synch}} \sim 10\%$ per day.

If we argue that the same amplitude of the synchrotron emission also occurs at the 1 cm wavelength and use this value in our simulations, it would give the lower limit of the flux variation due to synchrotron emission at 30 GHz of $\delta_{\text{synch}} \sim (T_b^{\text{synch}}/T_b)\Delta_{\text{synch}} \simeq 10^{-3}$, where T_b is the brightness temperature corresponding to the total planet flux and T_b^{synch} the one corresponding to the synchrotron emission. Thus, we can conclude that the variation of the

synchrotron emission at $\nu = 30$ GHz is not important for the antenna beam shape reconstruction for whole range of interest (≥ -60 dB). However, it is necessary to obtain additional observational data on the intrinsic atmospheric emission.⁷

Detailed studies by Goldin et al. (1997) of the millimeter and sub-millimeter spectra of Jupiter and Saturn have shown (see Fig. 8) that there are features in the spectra in this wavelength range. The two model spectra shown in Fig. 8 are from Griffin et al. (1986), using different physical conditions such as the size of NH_3 clumps, and the particle and gas scale heights ratio. Estimated temperatures of Jupiter and Saturn at the PLANCK corresponding observing frequencies are shown by filled diamond sign in Fig. 8. The first strong dip on both spectra almost coincide with the observing frequency 545 GHz near the 570 GHz NH_3 and PH_3 resonances. Estimated brightness temperatures with $\sim 10\%$ accuracy are given in Table 1 (see also Table 2).

Unfortunately, we do not have the information about variability of the Jupiter and Saturn fluxes in the range 30 to 857 GHz, which determines the accuracy of the beam shape reconstruction. Some naive expectation of the possible variability at the frequency range of interest at PLANCK could be related with the observed 20% deviations of Jupiter and Saturn temperature from the pure black body law $T(\nu) = \text{const}$. For Jupiter, this 20% deviation allows us to expect that some process, leading to such kind of variations, can be variable in time at the same level and have the characteristic time scale close to the period of Jupiter rotation (i.e. $\simeq 10$ hours). This problem needs an additional and more detailed investigation by using large ground-based radio telescopes in order to measure possible variation of Jupiter and Saturn fluxes at the PLANCK frequency range.

4.3. Expected polarization of the flux

One of the main goals of the PLANCK mission is the CMB polarization measurements. Firstly, we would like to point out that low limit of the polarization of Jupiter flux at 30 GHz exists, which is related to synchrotron emission.

According to Cortiglioni & Spoelstra (1992), the polarization level Π of synchrotron radiation is related to the spectral index β ($T_{\text{synch}} \propto \nu^\beta$) as

$$\Pi = \frac{3\beta + 3}{3\beta + 1}, \quad (19)$$

which gives $\sim 10 \div 75\%$ for various values of Π . The total polarized flux of Jupiter and Saturn is $\sim T_{\text{planet}}\Pi$. This fact creates pre-condition to use these planets for polarized antenna beam shape calibration.

Using the value $\beta = -1.26$ for $\nu > 13.6$ GHz for spectral index of the Jupiter synchrotron flux (Bolton et al.

⁷ We would like to argue that it is natural to expect non-zero fluctuation from the atmospheric emission. Partly our assumption is based on the millimeter and sub-millimeter spectrum of the atmospheric emission measurements at 30-857 GHz.

ν (GHz)	λ (mm)	beam (arcmin)	T_{Jupiter} (K)	T_{Saturn} (K)
30	10.00	33.0	152	133
44	6.82	24.0	158	135
70	4.29	14.0	167	138
100	3.00	10/9.2	173	141
143	2.10	7.1	176	144
217	1.38	5.0	179	146
353	0.85	5.0	178	141
545	0.55	5.0	133	118
857	0.35	5.0	145	114

Table 1. Brightness temperature T_b of Jupiter and Saturn at PLANCK observing frequencies with approximately 10% accuracy.

Planet	Date	Size (arcsec)	T_a (mK)				ecliptic Latitude	ecliptic Longitude	Distance from the Earth (AU)
			30	100	545 GHz	33'			
Jupiter	28.08.2007	38.6	40.04	455.9	1526	+0:26:30	250:31:33		5.0949
Saturn	04.12.2007	18.1	7.704	88.94	297.7	+1:34:10	158:14:46		9.1430
Jupiter	16.04.2008	39.2	41.30	511.8	1574	+0:00:11	291:26:07		5.0170
Saturn	16.05.2008	18.1	7.704	88.94	297.7	+1:46:03	151:43:16		9.1470
Jupiter	30.09.2008	39.7	42.35	525.0	1614	-0:19:28	283:12:00		4.9537
Saturn	17.12.2008	17.9	7.534	86.98	291.2	+1:58:58	171:27:11		9.2349
Jupiter	22.05.2009	40.4	43.86	556.3	1672	-0:45:33	325:59:50		4.8685
Saturn	31.05.2009	17.9	7.534	86.98	291.2	+2:07:48	164:57:29		9.2712

Table 2. Position of the planets on the dates of crossing by PLANCK on the ecliptic plane and antenna temperatures ($T_a = \Omega_{\text{planet}}/\Omega_{\text{beam}} \cdot T_b$) in transit via a scan angle.

2002), one obtain $\Pi_{\text{Jupiter}}=28\%$, indicating that the polarized part of the total flux can reach around 0.3% at the 1 cm wavelength range (see Table 2).

5. Effects from the strategy of the observations

5.1. Variations of the planet antenna temperatures versus distance to the planets

From the dates of crossing the scan angle by the planets, one can calculate the corresponding distance and hence the angular sizes of the planets. When the object size is sufficiently less than the solid angle of the beam, the antenna temperature T_a of the planet is given by

$$T_a = T_b \frac{\Omega_{\text{planet}}}{\Omega_{\text{beam}}} \quad (20)$$

where T_b is the brightness temperature of the planet (Table 1), Ω_{planet} the solid angle of the planet in observation (angular size in steradian), and Ω_{beam} the solid angle of the beam calculated with the simple approximation by the Gaussian shape

$$B = \exp\left(-\frac{\theta^2}{2\sigma^2}\right), \quad (21)$$

where $\sigma \equiv \sqrt{(\sigma_-^2 + \sigma_+^2)/2} = \theta_b/2.355$ and θ_b is the FWHM of the main beam. The results of calculation of the antenna temperatures for the three frequencies 30, 100 and 545 GHz with the corresponding FWHM sizes of 33, 10 and 5 arcmin are given in Table 2.

5.2. Scan strategy and peculiarities of the in-flight HFI beam reconstruction

In this subsection we would like to focus on the discussed scan strategy of the PLANCK mission and its influence on the in-flight antenna beam shape reconstruction using Jupiter and Saturn transits. According to the PLANCK mission requirement, the FWHM for the 10 LFI + HFI channels is shown in Table 1. Let us concentrate on the

beam shape properties above -30 dB for all LFI + HFI channels.

According to the scan strategy (see Fig.4), the orientation of the telescope spin axis during one hour (i.e. 1 r.p.m. of spin for 60 sub-scans) of observations should be stable: the orientation of the 60th sub-scan is parallel to that of the 1st sub-scan at the moment t_0 when a given circular scan starts to measure. At the end of the 60th sub-scan, the spin axis (and the optical axis) should change its orientation by $2.5'$ in the ecliptic plane (re-pointing). Thus, during Jupiter and Saturn transits the highest resolution scale from which the images of Jupiter and Saturn that can be recovered in the pixelized map is $2.5'$ in one side (as both the planets are less than $1'$).

Due to the pixelization scheme, however, we will face the following two situations at the higher frequency channels: the good case and the bad case of the planet transit. The good case is when the planets are caught by the beam peak just after re-pointing and have a maximum signal on a circular scan. The probability of such case is small. The bad case is when the planets bypass the beam maximum such that the point of maximum of the planet flux is missed by both of the neighbouring circular scans. In term of the map-making algorithm it means that the point of the maxima of Jupiter flux is formally shifted away from the center of the corresponding pixel and the signal at the surrounding pixels should have asymmetry. This asymmetry can be removed using the expected $10''$ pointing accuracy if there is no temporal variations in Jupiter flux or no mirror degradation effect.

Thus, the map-making algorithm should reflect directly the scan strategy and the position of Jupiter and Saturn (see Fig.1 and 4). Using -30 dB threshold we can estimate the number of pixels, which manifests the beam shape in the map for each frequency channel. For the simple Gaussian approximation (see Eq. (21)) we get

$$N_{\text{pix}}(\nu) \simeq 9 \left(\frac{\text{FWHM}(\nu)}{2.5'} \right)^2. \quad (22)$$

As one can see from Eq. (22), $N \sim 1570$ pixels in the 30 GHz channel ($\text{FWHM} \simeq 33'$), while $N \sim 36$ pixels only

for the 217 (and higher) GHz channels ($\text{FWHM} \simeq 5'$), which obviously is not enough to accurately determine these beam shape ellipticity, particularly if the ellipticity is no larger than 1.2.

6. Conclusions

In summary, regarding the issues related to using planet transit, such as Jupiter and Saturn, as a calibration method of the in-flight beam shape, we conclude the following:

- The high accuracy of the C_ℓ estimation by PLANCK will require the main beam estimation with error of 1%, which means that we need to measure the Jupiter variation $\delta B/B = \delta_S$ to the same level.
- For observations at the LFI frequency range, e.g. 30 \div 100 GHz, we have a limit of possible variation of the Jupiter flux ≤ 0.1 for the -30 dB threshold of the beam. In addition we need to measure the variation of Jupiter flux by using ground-based radio telescopes.
- For observations at high frequencies (217 \div 857 GHz), we can have problems during observation of the planets such as missing a target due to the narrow beams.
- Practically, during the mission (~ 15 months), we will be able to test the main beam about 3 times down to -23.5 dB by using Jupiter flux and 2 times by Saturn. This indicates that in the case of calibrating the beam degradation effect at intervals shorter than 3 months we have to use the method by Chiang et al. (2002a).
- The close (in time interval) transit of the planets will enable us to check a high-frequency component of the beam degradation.
- Neither planets, Jupiter and Saturn, are sufficient to test the far sidelobes.
- Galactic synchrotron and dust appear at the level of 0.18 mK.
- The possible degradation effect could be important at the same, as the Jupiter flux, level of variation $\sim 1 \div 10\%$ for the beam width.

We also note that the calibrations by Jupiter and Saturn, together with the method by Chiang et al. (2002a), allow one to restore the antenna beam shape for pixelized beam on the ΔT map, which is different from the antenna beam shape in the frame on the focal plane. In general cases, transition from the pixelized beam to the actual beam in the focal plane frame requires the knowledge about the noise properties (Chiang et al. 2002a).

Acknowledgment

This paper was supported in part by Danmarks Grundforskningsfond through its support for the establishment of the Theoretical Astrophysics Center, by a grant of RFBR 17625. The authors would like to thank C. Burigana, H. U. Norgaard-Nielsen and I. D. Novikov for useful discussions and S. Levin for useful remarks.

References

Bersanelli, M. & Lamarre, J.-M., 2001, PLANCK Systematic Effects Working Group: Objectives and Organisation, Technical Report ESA

Bolton, S. J., Janssen, M., Thorne, R., Levin, S., Klein, M., Gulkis, S., Bastian, T., Sault, R., Elachi, C., Hofstadter, M., Bunker, A., Dulk, G., Gudim, E., Hamilton, G., Johnson, W. T. K., Leblanc, Y., Liepack, O., McLeod, R., Roller, J., Roth, L., West, R., 2002, Nat, 415, 987

Burigana, C., Makaspina, M., Mandolesi, N., Danese, L., Maino, D., Bersanelli, M., Maltoni, M., 1997, Internal report ITESRE 198/1997 (astro-ph/9906360).

Burigana C., Natoli P., Vittorio N., Mandolesi N., Bersanelli M. 2001, Experimental Astron. 12, 87

Burke, B.F., Franklin, K.L., 1955, J. Geophys. Res. 60, 213

Chiang, L.-Y., Christensen, P.R., Jørgensen, H.E., Naselsky, I.P., Naselsky, P.D., Novikov, D.I., Novikov, I.D., 2002a, A&A, 392, 369

Chiang, L.-Y., Jørgensen H.E., Naselsky I.P., Naselsky P.D., Novikov I.D., Christensen P.R., 2002b, MNRAS, 335, 1054

Cortiglioni, S., & Spoelstra, T. A. T., 1995, A&A, 302, 1

De Maagt, P., Polegre, A. M., & Crone, G., 1998, PLANCK – Straylight Evaluation of the Carrier Configuration, Technical report ESA, PT-TN-05967, 1/0

Downey, E.C., 2002. XEphem Version 3.5.2, <http://www.clearskyinstitute.com/xephem/xephem.html>

Goldin, A. B., Kowitt, M. S., Cheng, E. S., Cottingham, D. A., Fixsen, D. J., Inman, C. A., Meyer, S. S., Puchalla, J. L., Ruhl, J. E., Silverberg, R. F., 1997 ApJ, 488, L161

Griffin, M.J., Ade, P.A.R., Orton, G.S., Robson, E.I., Gear, W.K., Nolt, I.G., Radostitz, J.V., 1986, Icarus, 65, 244

Gurnett, D.A., Kurth, W.S., Hospodarsky, G.B., Persoon, A.M., Zarka, P., Lecacheux, A., Bolton, S.J., Desch, M.D., Farrell, W.M.; Kaiser, M.L.; Ladreiter, H.-P.; Rucker, H.O.; Galopeau, P., Louarn, P., Young, D.T., Pryor, W.R., Dougherty, M.K. 2002. Nat, 415, 985

Mandolesi, N. et al. 1998, PLANCK Low Frequency Instrument, A Proposal Submitted to ESA

Mandolesi, N., et al. 2000, Astro. Lett. Comm., 37, 151

Puget, J. L., et al. 1998, High Frequency Instrument for the PLANCK Mission, A Proposal Submitted to ESA

Tegmark M., 1996, ApJ, 470, 81

Wu, J. H. P. et al., 2001, ApJS, 132, 1